ANAMET Report 045
July 2004

The Uncertainty of the "Direct Method" for measuring the equivalent source mismatch of a power splitter:
A case study in using software for uncertainty calculation

B Hall and M Rodriguez

ANAMET reports are produced by, and for, the members of ANAMET. They are intended for fast dissemination of technical information for discussion purposes and do not necessarily represent an official viewpoint. No responsibility is accepted by the author(s) or ANAMET for any use made of the information in this report.

For further information about ANAMET and its activities contact:

Internet: **http://www.npl.co.uk/npl/clubs/anamet/index.html**

E-mail: **anamet@npl.co.uk**

Comments on this report should be sent to :

Mail: ANAMET
Division of Enabling Metrology
National Physical Laboratory
Queens Road
Teddington
Middlesex
TW11 0LW

Fax: 020 8943 6098 (UK)
+ 44 20 8943 6098 (International)

This report has been approved by the ANAMET Steering Committee

Report Draft

The uncertainty of the 'Direct Method' for measuring the equivalent source mismatch of a power splitter:

A case study in using software for uncertainty calculation

Blair Hall,
Measurement Standards Laboratory of New Zealand,
PO Box 31-310,
Lower Hutt, New Zealand.

Manuel Rodríguez,
RF & Microwave Laboratory
INTA -Área de Metrología y Calibración
Ctra. a Ajalvir, p.k. 4
28850 Torrejón de Ardoz, Spain.

April 21, 2004

Abstract

This work was carried out as a 'case study' in applying new techniques for propagating uncertainty in complex-valued quantities (N. M. Ridler and M. J. Salter, Metrologia, **39** (2002) 295-302). The method was applied, using special software to handle the calculations, to the analysis of data characterising a resistive power splitter (Weinschel, model 1870A). The data used in the study was collected at INTA (Spain) and analysed at MSL (New Zealand).

The study also investigated a modelling approach to vector network analyser (VNA) measurement uncertainty. A signal flow model of a VNA was used to assign uncertainty to raw measurements. The model parameters were based on measured performance figures of the VNA system (they allow for the inherent sources of uncertainty, such as noise, cable and connector repeatability, etc). The study presents these, model-based, uncertainties together with an independent estimate of uncertainties based on the sample statistics of a small number repeated measurements.

The study used the so-called 'Direct Method' to characterise splitter output ports (J. R. Juroshek, Microwave J., **10** (1997) 106-118). The method determines three complex parameters for a port. In particular, the equivalent source mismatch, and an associated scalar quantity, the effective voltage standing wave ratio, are reported on in detail.

The parameters obtained by the Direct Method can be used to correct for linear systematic errors in reflection measurements, allowing the splitter, connected to a VNA, to be used as a reflectometer. The study uses this possibility to compare the voltage reflection coefficient of a known termination with independently traceable values.

The study reports uncertainty calculations for these measurements, using the two alternative estimates of input uncertainties. It concludes that formal propagation of uncertainty is feasible in this kind of experiment. Fair agreement was found between both methods used to estimate input uncertainties. In particular, the measurement comparisons made on the 50 dB attenuator are satisfactory for both methods.

Contents

1 Introduction

This study has applied new techniques for propagation of uncertainty in complex-valued quantities to raw measurement data, obtaining statements of uncertainty for the results that can be traced back to the uncertainties in quantities influencing the measurement [1]. The treatment of uncertainties in complex-valued measurements has yet to be harmonized, as it has been for scalar measurements by the ISO-published *Guide to the expression of uncertainty in measurement* [2]. The new approach follows the spirit of recommendations in the *Guide*, but applies mathematical techniques suitable for complex-valued quantities (which the *Guide* does not cover).

The main reason for undertaking this work has been to gain experience in applying the formal mathematical procedure for propagating uncertainty. The work represents a 'case study', looking at the practicality of the approach and the consistency of the results obtained.

Although the mathematical procedure is clear, there are many steps involved and it can be difficult to keep track of individual contributions. Accordingly, the study has used special software to perform the uncertainty calculations. The software is novel and very effective at simplifying the task of data processing. It is discussed briefly in this report, with ample references provided for further information.

A series of measurements were used to characterise a resistive power splitter output port, following the so-called 'Direct Method' [3]. The method estimates three complex parameters for a port, which can be considered to correct the equivalent network for linear errors, so that a calibrated port can be used as a reflectometer, to measure complex voltage reflection coefficients (VRC). We report in some detail on one of the three parameters, the equivalent source mismatch, and an associated scalar quantity, the effective voltage standing wave ratio.

The basic idea underlying this study is that the set of parameters characterising a splitter port, together with uncertainties, can be calculated according to the method described in [1]. The calculations involve measured reflection data from a set of calibration standards and the corresponding 'certified' values for the standards.[1] All these 'inputs' to the calculation are uncertain in value. These uncertainties propagate to the output parameters, which in general are correlated. A calibrated port can be used for reflection measurements, by applying a correction to raw measurements based on the port parameters. Full uncertainty statements are obtained by propagating the parameter uncertainties through the correction equation.

It is possible to check the correctness of the calculated uncertainties by making measurements of a known item. In this case, the VRC of a 50 dB attenuator was measured and compared with corresponding NPL-certified values. Over a series of independent measurements, the observed differences are indicative of the accuracy of the calculated uncertainties. For instance, when uncertainty regions are evaluated

[1] A set of NPL-calibrated standards were available.

at a level of confidence of 95%, it is to be expected that, on average, one in twenty will not include the measurand.[2]

The study has also investigated the possibility of modelling the measurement uncertainty contribution of a vector network analyser (VNA). We have assigned uncertainties to raw VNA measurements that are based on a number of measured VNA performance data. The strict mathematical framework for uncertainty propagation makes this approach possible, using software to perform the calculations. To evaluate the modelling accuracy, a second, independent, method of estimating the uncertainty in the raw measurements was also used. This method based uncertainty estimates on the sample variance of a small set of repeated measurements (i.e., a Type A uncertainty estimate of the measurements).

The remainder of the Introduction covers the notation used in mathematical expressions, a summary of the method for propagating uncertainty and an overview of the special software techniques used. Section 2 describes details of the experiment and experimental procedures used. Section 3 then presents the results of the study. Several appendices are provided: Appendix A describes our signal flow model of the contributions to uncertainty in a vector network analyser measurement, Appendix B describes the algorithm used to calculate an effective number of degrees-of-freedom for results, and Appendix C presents extensions to the notions of sensitivity coefficients and components of uncertainty for complex-value uncertainty calculations, and then applies them to some of the results in this study.

1.1 Notation

Complex quantities are written in bold italic type (e.g., $\boldsymbol{x}, \boldsymbol{S}$). When referring to the scalar components of a complex quantity, subscripts '1' and '2' are used; '1' labels the real component and '2' the imaginary (e.g., $\boldsymbol{x} = x_1 + \mathrm{j}\, x_2.$).

Vectors and matrices are written in bold Roman capitals (e.g., $\mathbf{M}$) and a prime indicates the matrix transpose (e.g., $\mathbf{M}'$). To identify the scalar components of a complex vector, extra subscripts ('1' and '2') are placed in front of the subscript for the particular vector element. For example, the elements of a column vector of m complex elements can be identified as

$$[\boldsymbol{x}_1, \boldsymbol{x}_2, \cdots, \boldsymbol{x}_m]' \Leftrightarrow [x_{11}, x_{21}, x_{12}, x_{22}, \cdots, x_{1m}, x_{2m}]' \ . \tag{1}$$

1.2 Propagation of uncertainty in complex quantities

This section reviews the method of propagating uncertainty in complex quantities outlined in Section 8 of [1]. In this summary, single, rather than multiple, output

[2] Although such a check does not *guarantee* the correctness of the uncertainties, it provides an opportunity to spot problems. For instance, uncertainties that are grossly too small or too large should be obvious.

quantities are considered and a slightly different notation is used, otherwise the approach is the same.

An arbitrary measurement function

$$\boldsymbol{y} = \boldsymbol{f}(\mathbf{X}) = \boldsymbol{f}(\boldsymbol{x}_1, \boldsymbol{x}_2, \cdots, \boldsymbol{x}_m) \,, \tag{2}$$

describes the relation between a complex-valued quantity of interest, $\boldsymbol{y}$ – the measurand, and m influence quantities on which it depends. The function $\boldsymbol{f}$ comprises two scalar functions, f_1 and f_2, that evaluate the real and imaginary components respectively (i.e., $\boldsymbol{y} = f_1(\mathbf{X}) + \mathrm{j}\, f_2(\mathbf{X})$).

The uncertainty in the values assigned to input quantities is represented by a $2m \times 2m$ covariance matrix,

$$\mathbf{V}(\mathbf{X}) = \begin{bmatrix} u^2(x_{11}) & u(x_{11}, x_{21}) & \cdots & u(x_{11}, x_{1m}) & u(x_{11}, x_{2m}) \\ u(x_{21}, x_{11}) & u^2(x_{21}) & \cdots & u(x_{21}, x_{1m}) & u(x_{21}, x_{2m}) \\ \vdots & \vdots & \ddots & \vdots & \vdots \\ u(x_{1m}, x_{11}) & u(x_{1m}, x_{21}) & \cdots & u^2(x_{1m}) & u(x_{1m}, x_{2m}) \\ u(x_{2m}, x_{11}) & u(x_{2m}, x_{21}) & \cdots & u(x_{2m}, x_{1m}) & u^2(x_{2m}) \end{bmatrix} \,, \tag{3}$$

where the diagonal terms $u^2(x_{ij})$ are standard variances of the associated inputs x_{ij} and the $u(x_{ij}, x_{kl})$ terms, off the diagonal, represent the covariance between x_{ij} and x_{kl}.

The uncertainty in $\boldsymbol{y}$ is expressed in a (2×2) covariance matrix

$$\mathbf{V}(\boldsymbol{y}) = \mathbf{J}(\boldsymbol{y})\, \mathbf{V}(\mathbf{X})\, \mathbf{J}(\boldsymbol{y})' \,, \tag{4}$$

where $\mathbf{J}(\boldsymbol{y})$ is the $2 \times 2m$ Jacobian matrix of the partial derivatives of the scalar components of $\boldsymbol{f}$ with respect to the scalar elements of $\mathbf{X}$,

$$\mathbf{J}(\boldsymbol{y}) = \begin{bmatrix} \frac{\partial f_1}{\partial x_{11}} & \frac{\partial f_1}{\partial x_{21}} & \frac{\partial f_1}{\partial x_{12}} & \frac{\partial f_1}{\partial x_{22}} & \cdots & \frac{\partial f_1}{\partial x_{1m}} & \frac{\partial f_1}{\partial x_{2m}} \\ \frac{\partial f_2}{\partial x_{11}} & \frac{\partial f_2}{\partial x_{21}} & \frac{\partial f_2}{\partial x_{12}} & \frac{\partial f_2}{\partial x_{22}} & \cdots & \frac{\partial f_2}{\partial x_{1m}} & \frac{\partial f_2}{\partial x_{2m}} \end{bmatrix} \,. \tag{5}$$

1.3 Software

This study adheres to the mathematical principles presented above, however, by using special software it is actually possible to avoid an explicit formulation of the problem in terms of a single 'measurement function', $\boldsymbol{f}$, and to construct a full variance-covariance matrix for the input quantities, as in equation (3). These requirements are difficult in practice.

Instead, the analysis has been carried out in software directly in terms of a series measurement equations describing steps in the measurement procedure. The underlying uncertainty calculations are handled automatically by the software, so there is no need to even differentiate the measurement equations to obtain sensitivity coefficients.

A novel construct is used to represent measurement results, called an *uncertain number*. It is a concise and elegant notion that encapsulates all the attributes of a measurement result: value, uncertainty, degrees-of-freedom, etc. Software can be designed to take care of most of the 'hard work' of uncertainty calculations using this technique [5].

An implementation of uncertain numbers introduces a new 'abstract data type' to a particular programming langauge.[3] When uncertain numbers are used in measurement functions, the software looks like an expression for the measurement result. However, as a side-effect, the associated uncertainty calculations are performed automatically. The uncertain number resulting from a calculation encapsulates the full measurement result, including the uncertainty.

For example, the actual source code for equation (7), of Section 2.2, looks like[4]

```
def correct(self,gamma,f):
    num = gamma[f]-self._Ed[f]
    den = self._Es[f] * num + self._Er[f]
    return num / den
```

Without going into detail, it is important to note that this code is simply an implementation of equation (7); it does not describe the partial derivatives as well. The associated uncertainty expressions are algorithmically deduced from the measurement equation – something the uncertain number package software is designed to do.[5] A more impressive example is perhaps the solution of equation (9), in Section 2.3, which uses an LU-decomposition algorithm from linear algebra to solve a set of linear equations. That souce code is

```
def onePort(measure, artefact):

    H =  [ (gamma,1.0,-gamma * gamma_m)
                for (gamma,gamma_m) in zip(artefact,measure) ]

    ABC = LU.solve( Numeric.array(H), Numeric.array(measure) )

    E_D = ABC[1]
    E_S = -ABC[2]
    E_R = ABC[0] + E_D * E_S

    return Numeric.array( (E_D, E_S, E_R) )
```

This function evaluates three complex error correction terms $\boldsymbol{E}_{\mathrm{D}}$, $\boldsymbol{E}_{\mathrm{S}}$ and $\boldsymbol{E}_{\mathrm{R}}$, which

[3] A regular software 'type', like an `integer` or `float`, is defined as part of a programming language. Object-oriented languages generalise the notion of type to allow programmers to design their own. For example, C++ does not have a native complex-number type, but one is provided in a standard library. The rules of complex arithmetic and simple functions are a part of its definition. So, when complex arithmetic operations occur, the underlying manipulation of real and imaginary components is handled implicitly. Uncertain numbers are similar: the low-level manipulations involved in uncertainty propagation are part of the type-definition, relieving programmers of that level of detail.

[4] This function is part of a Python class definition. The name `self` refers to a class instance.

[5] Neither symbolic differentiation nor finite-difference methods are used. The technique is rather easier, yet it is accurate to within the limits of machine round-off.

are calculated from a sequence of three uncertain numbers for measured values, in `measure`, and three uncertain numbers for standards' values, in `artefact`. The triplet returned, `(E_D, E_S, E_R)`, consists of uncertain numbers with the appropriate uncertainty attributes. The function `LU.solve` is just an implementation of a standard LU decomposition algorithm [6].

The code snippets above are written in Python, which was used to write many short, problem-specific, routines for data entry, data manipulation and data presentation in this study.[6] These routines rely on a general-purpose software package for complex uncertainty calculations [7]. The documentation for the package contains several annotated examples of one-port calibration.

2 Experimental details

2.1 Raw measurements

The raw data for this study was collected at INTA. The measurements were originally made during the ANAMET 022 measurement comparison.

An HP8510C network analyser was used to measure a Weinschel, model 1870A, two-resistor power splitter with female N-type RF connectors. The open, short and broadband load used for the Direct Method were all calibrated at NPL. The reflection coefficient of a 50 dB attenuator, also measured at NPL, was used as a verification standard. NPL calibration certificates contain information sufficient to assign a covariance matrix to the estimated value of each item. They also report a coverage factor for a 95% region of uncertainty, which can be used to assign a number of degrees-of-freedom by applying the inverse of equation (10), in Section 3.1.

The ANAMET 022 comparison protocol requires participants to measure ports 2 and 3 of the splitter, so the Direct Method was applied to each port to measure the equivalent source mismatch. Measurements were repeated three times (including reconnection), so the raw data consisted of 18 measurements for each port (3 standards $\times$ 2 $\boldsymbol{S}$-parameters $\times$ 3 repeats). In addition, 3 repeat measurements of the 50 dB attenuator connected to the free splitter port were made.

Measurements were performed at intervals of 1 GHz, from 1 GHz to 18 GHz.

2.2 The Direct Method

The Direct Method was first suggested by John Juroshek, of NIST [3]. It is a convenient way of measuring the equivalent source mismatch of a 3-port coupler using a VNA and a set of 1-port calibration standards.

[6] We do not expect the data-specific routines to be of interest, because they depend very much on file formats and other legacy software. However, listings are available on request.

Briefly, two of the coupler ports are connected directly to the VNA, leaving the remaining port 'free'. This port is then 'calibrated' as a reflectometer, by measuring the various standards and applying the usual mathematical procedure.[7]

The Direct Method can use an uncalibrated vector network analyser (VNA), so the contributions to VNA uncertainty are essentially those due to inherent instrument imperfections and noise.

The Direct Method determines a triplet of linear 'error correction' terms for the splitter port: $\boldsymbol{E}_{\mathrm{D}}$, the directivity; $\boldsymbol{E}_{\mathrm{S}}$, the source match; $\boldsymbol{E}_{\mathrm{R}}$ and the reflection tracking. These are often represented as the elements of an error adaptor network, as shown in the signal flow diagram of Figure 1.

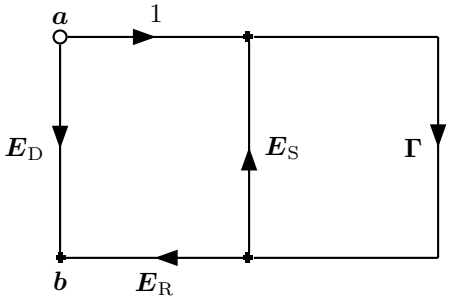

Figure 1: The error-adaptor network of a reflectometer. When a component with a reflection coefficient $\boldsymbol{\Gamma}$ is connected to the calibrated port on the right, the reflection coefficient, $\boldsymbol{\Gamma}^{\mathrm{m}} = \boldsymbol{b}/\boldsymbol{a}$, measured on the left will include the effects of the adaptor network.

In principle, a calibrated splitter port can be used as a 1-port reflectometer if the systematic effects of the network are corrected for. The reflection measurement is

$$\boldsymbol{\Gamma}^{\mathrm{m}} = \frac{\boldsymbol{b}}{\boldsymbol{a}} = \boldsymbol{E}_{\mathrm{D}} + \frac{\boldsymbol{\Gamma}\boldsymbol{E}_{\mathrm{R}}}{1 - \boldsymbol{\Gamma}\boldsymbol{E}_{\mathrm{S}}} \,. \tag{6}$$

So, working backwards, an estimate can be found for the reflection coefficient of interest

$$\hat{\boldsymbol{\Gamma}} = \frac{\boldsymbol{\Gamma}^{\mathrm{m}} - \boldsymbol{E}_{\mathrm{D}}}{\boldsymbol{E}_{\mathrm{R}} + \boldsymbol{E}_{\mathrm{S}}\left(\boldsymbol{\Gamma}^{\mathrm{m}} - \boldsymbol{E}_{\mathrm{D}}\right)} \,. \tag{7}$$

The ANAMET 022 comparison protocol asks for values of effective voltage standing wave ratio (VSWR) of $\boldsymbol{E}_{\mathrm{S}}$, which is scalar. The VSWR of a complex reflection coefficient $\boldsymbol{\Gamma}$ is

$$\mathrm{VSWR}(\boldsymbol{\Gamma}) = \frac{1 + |\boldsymbol{\Gamma}|}{1 - |\boldsymbol{\Gamma}|} \,. \tag{8}$$

2.3 One-port calibration

The so-called 'Open-Short-Load' calibration procedure was used in conjunction with the Direct Method. Measurements were made of an open, short and load, then a set

[7] During calibration, *ratios* of raw VNA measurements, $\boldsymbol{S}_{11}/\boldsymbol{S}_{21}$, are used in the 1-port calibration calculations.

of simultaneous equations were solved to extract the parameters $\boldsymbol{E}_{\mathrm{D}}$, $\boldsymbol{E}_{\mathrm{S}}$ and $\boldsymbol{E}_{\mathrm{R}}$ that characterise the splitter port.

The mathematical treatment is as follows. The calibrated values of the standards are denoted $\boldsymbol{\Gamma}_1$, $\boldsymbol{\Gamma}_2$ and $\boldsymbol{\Gamma}_3$ and the corresponding measured values[8] $\boldsymbol{\Gamma}_1^{\mathrm{m}}$, $\boldsymbol{\Gamma}_2^{\mathrm{m}}$ and $\boldsymbol{\Gamma}_3^{\mathrm{m}}$. The complex parameters $\boldsymbol{A}$, $\boldsymbol{B}$ and $\boldsymbol{C}$ are found by solving the equations

$$\begin{bmatrix} \boldsymbol{\Gamma}_1 & 1 & -\boldsymbol{\Gamma}_1^{\mathrm{m}}\boldsymbol{\Gamma}_1 \\ \boldsymbol{\Gamma}_2 & 1 & -\boldsymbol{\Gamma}_2^{\mathrm{m}}\boldsymbol{\Gamma}_2 \\ \boldsymbol{\Gamma}_3 & 1 & -\boldsymbol{\Gamma}_3^{\mathrm{m}}\boldsymbol{\Gamma}_3 \end{bmatrix} \begin{bmatrix} \boldsymbol{A} \\ \boldsymbol{B} \\ \boldsymbol{C} \end{bmatrix} = \begin{bmatrix} \boldsymbol{\Gamma}_1^{\mathrm{m}} \\ \boldsymbol{\Gamma}_2^{\mathrm{m}} \\ \boldsymbol{\Gamma}_3^{\mathrm{m}} \end{bmatrix} . \tag{9}$$

and then the error terms are given by

$$\begin{aligned} \boldsymbol{E}_{\mathrm{D}} &= \boldsymbol{B} , \\ \boldsymbol{E}_{\mathrm{S}} &= -\boldsymbol{C} , \\ \boldsymbol{E}_{\mathrm{R}} &= \boldsymbol{A} - \boldsymbol{B}\boldsymbol{C} . \end{aligned}$$

3 Results

The numerical results in this study relate to the uncertainties calculated for the measured values. These were obtained using the procedure for propagating uncertainties described in Section 1.2. However, for each measurement we have used two independent estimates of input uncertainty. So, for each measurement result, there are two uncertainties reported. As explained in the Introduction, our reason for doing this was to investigate the possibility of modelling VNA uncertainty. We have developed a model of the signal flow within a VNA (see Appendix A) and used certain VNA performance measures to quantify its elements. This model was used to assign uncertainty to raw VMA measurements. The alternative method of assigning uncertainty to measured values used a simple type A assessment of three repeated measurements (i.e., the covariance of the sample mean was associated with the input quantity). In presenting the results associated with these two alternatives, we refer to the former as 'model' and the latter as 'type A'.

Unfortunately, it is not possible to be rigorous in the comparison of uncertainties in this study, because there are too few measurements involved.[9] However, we can consider the following questions:

- Do the results indicate that the propagated uncertainties are accurate?
- Do either, or both, methods of estimating input uncertainty appear to be satisfactory?

[8] A measured value $\boldsymbol{\Gamma}^{\mathrm{m}}$ for a given standard is actually the ratio of two raw VNA scattering measurements, $\boldsymbol{S}_{11}/\boldsymbol{S}_{21}$.

[9] The comparison of statements of uncertainty is a subtle problem. In principle, it is the *procedure* for calculating uncertainties that should be scrutinized, because two alternative, albeit *correct*, procedures can produce different uncertainty intervals for a particular measurement result. The *correctness* of a procedure for estimating uncertainty must be tested over many repeated (independent) measurements to see if the stated level of confidence is achieved.

The results presented in the remainder of this section suggest that indeed both methods of uncertainty assessment are performing adequately, although there may be a few problems associated with the very small sample of repeated measurements ($N = 3$).[10] Significantly, the results give every indication that uncertainties are being propagated accurately through the various measurement equations involved, which supports the underlying mathematical method used (Section 1.2) and the associated software.

3.1 Notes about presentation

To ease comparison and interpretation of the results, covariance matrices are reduced below to single summary values. In general, uncertainty can be represented by an elliptical region-of-uncertainty, whose shape is determined by the covariance matrix of a result. This ellipse is scaled by a **coverage factor** that depends on the effective degrees-of-freedom [1]. To simplify reporting, we adopt a *circular* region centered around the measurement result that *approximates* the extent of the actual elliptical region-of-uncertainty.[11] Then the **expanded uncertainty**, U, is defined as the radius of this *circular* region. All expanded uncertainties are calculated to approximate a level of confidence of 95%.

Because U does not convey any information about the shape of the elliptical region of uncertainty, we also calculate the **eccentricity**,

$$e = \sqrt{1 - \frac{b^2}{a^2}} \ ,$$

where b is the semiminor axis and a is the semimajor axis of the actual region of uncertainty. When $e = 0$, the region is a circle.

The **coverage factor**, k, scales the region of uncertainty to provide the required level of confidence. It depends only on the number of degrees-of-freedom:

$$k = \sqrt{\frac{2\nu}{\nu - 1} F_{2,\nu-1,0.95}} \ , \tag{10}$$

where ν is the number of degrees-of-freedom and $F_{2,\nu-1,0.95}$ is the 95% point of the F-distribution with degrees-of-freedom parameters 2 and $\nu - 1$. When $\nu = \infty$, $k = 2.45$.

3.2 Effective source match

Expanded uncertainties for measurements of the effective source mismatch, $\boldsymbol{E}_{\mathrm{S}}$, at splitter port 2 are shown in Fig. 2, the corresponding numerical data is reported

[10] For complex measurements, a sample size of three is the smallest for which the degrees-of-freedom can be handled. Earlier work has shown that the coverage factors for samples with $N = 3$ are very large and that there is a bias to calculate conservative uncertainty regions [8].

[11] The areas of the circle and the ellipse are actually the same. However, more importantly, this means the Total Variance associated with the respective covariance matrices is the same [4].

in Tables 1 and 2, together with the calculated value, the eccentricity, effective degrees-of-freedom and the coverage factor. This data is essentially a copy of the screen output from the computer – a little editing has been done to make things easier to read.

The agreement between the two sets of expanded uncertainties is very good. The uncertainties calculated using the model are slightly more conservative than the type A assessment.

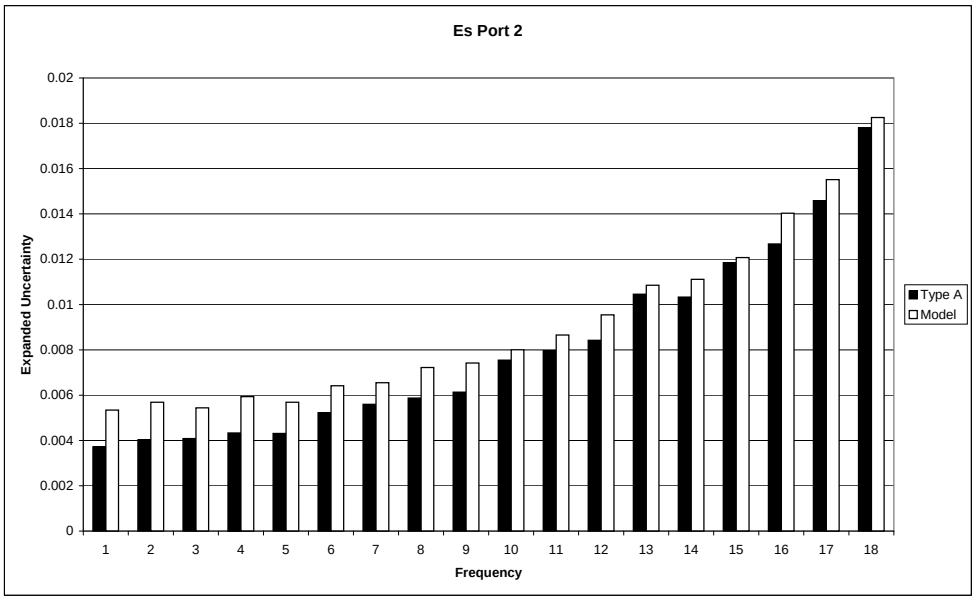

Figure 2: Effective source match values for port 2.

Table 1: $\boldsymbol{E}_{\mathrm{S}}$ at splitter port 2: type A uncertainties.

f	real + j imag	U	e	dof	k
1	0.002062 + j 0.005919	0.003718	0.08	269	2.47
2	0.007390 + j -0.001857	0.004025	0.16	224	2.47
3	0.001315 + j -0.006977	0.004086	0.33	134	2.49
4	-0.007258 + j -0.000106	0.004331	0.30	79	2.51
5	-0.006130 + j 0.009970	0.004307	0.31	65	2.53
6	0.005736 + j 0.012035	0.005223	0.44	38	2.58
7	0.011594 + j 0.003071	0.005597	0.52	33	2.61
8	0.007224 + j 0.001060	0.005869	0.17	24	2.68
9	0.004795 + j 0.007536	0.006133	0.29	24	2.68
10	0.006680 + j 0.018923	0.007547	0.55	21	2.71
11	0.008424 + j 0.017808	0.007960	0.36	16	2.80
12	0.011950 + j 0.019399	0.008419	0.30	15	2.86
13	0.012746 + j 0.014970	0.010459	0.57	14	2.90
14	0.009814 + j 0.011363	0.010328	0.40	15	2.86
15	0.003794 + j 0.011580	0.011839	0.42	16	2.83
16	-0.001849 + j 0.022133	0.012672	0.16	14	2.86
17	0.002510 + j 0.033009	0.014579	0.33	14	2.86
18	0.005106 + j 0.020030	0.017803	0.32	13	2.94

Table 2: $\boldsymbol{E}_{\mathrm{S}}$ at splitter port 2: model uncertainties.

f	real + j imag	U	e	dof	k
1	0.002062 + j 0.005919	0.005339	0.00	892	2.45
2	0.007390 + j -0.001857	0.005685	0.00	740	2.45
3	0.001315 + j -0.006977	0.005441	0.00	485	2.46
4	-0.007258 + j -0.000106	0.005935	0.00	304	2.46
5	-0.006130 + j 0.009970	0.005684	0.00	214	2.47
6	0.005736 + j 0.012035	0.006418	0.00	152	2.48
7	0.011594 + j 0.003071	0.006550	0.00	98	2.50
8	0.007224 + j 0.001060	0.007220	0.00	69	2.52
9	0.004795 + j 0.007536	0.007420	0.00	65	2.53
10	0.006680 + j 0.018923	0.008005	0.00	45	2.56
11	0.008424 + j 0.017808	0.008656	0.00	31	2.62
12	0.011950 + j 0.019399	0.009541	0.00	37	2.59
13	0.012746 + j 0.014970	0.010850	0.00	35	2.60
14	0.009814 + j 0.011363	0.011114	0.00	31	2.62
15	0.003794 + j 0.011580	0.012070	0.00	25	2.67
16	-0.001849 + j 0.022133	0.014028	0.00	32	2.61
17	0.002510 + j 0.033009	0.015514	0.00	25	2.66
18	0.005106 + j 0.020030	0.018253	0.00	19	2.74

Figure 3 shows expanded uncertainties for $\boldsymbol{E}_{\mathrm{S}}$ values at splitter port 3. The numerical data is reported in Tables 3 and 4.

Here, we note a distinct difference between the type A and the model data, apparent above about 6 GHz. The larger U values in the type A data can be attributed to more scatter in the sample statistics. In Table 3, there is a correlation between the larger expanded uncertainties and smaller numbers of degrees-of-freedom. This suggests an increase in the relative importance of the type A uncertainty contributions in these measurements. The values of eccentricity are also a bit larger, indicating a more elliptical shape for the region of uncertainty (see also Appendix C.3).

The model-based expanded uncertainties cannot, of course, reproduce the same trend, because it is based on the scatter in the three repeated measurements at each point. Further investigation would be required to decide whether some of the model-based uncertainty contributions are actually too optimistic. It is equally possible that a small problem occurred with these measurements, or that the very small sample size may give rise to fluctuations like this.[12]

It is notable that the effect did not appear at the other port, where the model uncertainties appeared conservative for the measurements.

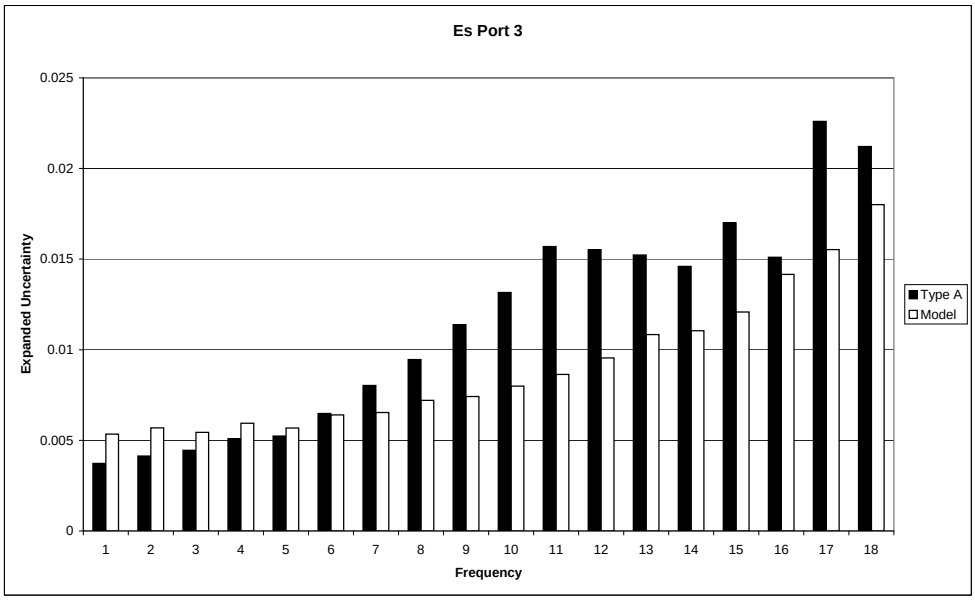

Figure 3: Effective source match values for port 3.

[12]The observed discrepancy is typical of the problems one faces when trying to compare different procedures for evaluating uncertainty. We see here that in one case the type A dominates but in another the model uncertainties are bigger. Which is correct – which is wrong!? The reality may be that both *procedures* are doing a good job. We have seen only a few results, but on average, over many different experiments, the apparent differences may be insignificant.

Table 3: $\boldsymbol{E}_{\mathrm{S}}$ at splitter port 3: type A uncertainties.

f	real + j imag	U	e	dof	k
1	0.001679 + j 0.006558	0.003729	0.14	270	2.47
2	0.006912 + j -0.000083	0.004134	0.34	187	2.47
3	0.002215 + j -0.006065	0.004451	0.50	58	2.54
4	-0.006240 + j -0.001861	0.005085	0.56	39	2.58
5	-0.005950 + j 0.006578	0.005238	0.51	29	2.63
6	0.005559 + j 0.008311	0.006479	0.60	18	2.76
7	0.012425 + j -0.001789	0.008029	0.65	14	2.86
8	0.006796 + j -0.004475	0.009461	0.76	11	3.00
9	0.001847 + j 0.007102	0.011376	0.83	9	3.28
10	0.007844 + j 0.025153	0.013154	0.77	9	3.17
11	0.019537 + j 0.020774	0.015689	0.88	7	3.45
12	0.018169 + j 0.008990	0.015519	0.86	8	3.44
13	-0.001060 + j 0.002327	0.015223	0.79	9	3.16
14	-0.012157 + j 0.020251	0.014594	0.72	11	3.00
15	0.002309 + j 0.034860	0.016996	0.74	10	3.07
16	0.023330 + j 0.028785	0.015099	0.68	15	2.86
17	0.020755 + j 0.002736	0.022598	0.75	11	3.07
18	-0.006684 + j -0.007784	0.021212	0.57	15	2.83

Table 4: $\boldsymbol{E}_{\mathrm{S}}$ at splitter port 3: model uncertainties.

f	real + j imag	U	e	dof	k
1	0.002062 + j 0.005919	0.005339	0.00	892	2.45
2	0.007390 + j -0.001857	0.005685	0.00	740	2.45
3	0.001315 + j -0.006977	0.005441	0.00	485	2.46
4	-0.007258 + j -0.000106	0.005935	0.00	304	2.46
5	-0.006130 + j 0.009970	0.005684	0.00	214	2.47
6	0.005736 + j 0.012035	0.006418	0.00	152	2.48
7	0.011594 + j 0.003071	0.006550	0.00	98	2.50
8	0.007224 + j 0.001060	0.007220	0.00	69	2.52
9	0.004795 + j 0.007536	0.007420	0.00	65	2.53
10	0.006680 + j 0.018923	0.008005	0.00	45	2.56
11	0.008424 + j 0.017808	0.008656	0.00	31	2.62
12	0.011950 + j 0.019399	0.009541	0.00	37	2.59
13	0.012746 + j 0.014970	0.010850	0.00	35	2.60
14	0.009814 + j 0.011363	0.011114	0.00	31	2.62
15	0.003794 + j 0.011580	0.012070	0.00	25	2.67
16	-0.001849 + j 0.022133	0.014028	0.00	32	2.61
17	0.002510 + j 0.033009	0.015514	0.00	25	2.66
18	0.005106 + j 0.020030	0.018253	0.00	19	2.74

3.3 Voltage standing wave ratio

Expanded uncertainties for values of the voltage standing wave ratio (VSWR), at splitter port 2 are shown in Fig. 4, the corresponding numerical data is reported in Tables 5 and 6, together with the calculated value, effective degrees-of-freedom and the k factor. Note that VSWR is a scalar quantity, so the expanded uncertainties in this section are calculated according to the *Guide* and the k factor is determined from the Student t-distribution, etc.

The port 2 VSWR results show no significant differences between the two methods. If anything, the model-based calculations give a slightly more conservative uncertainty estimate, as was the case for the $\boldsymbol{E}_{\mathrm{S}}$ measurements at the same port.

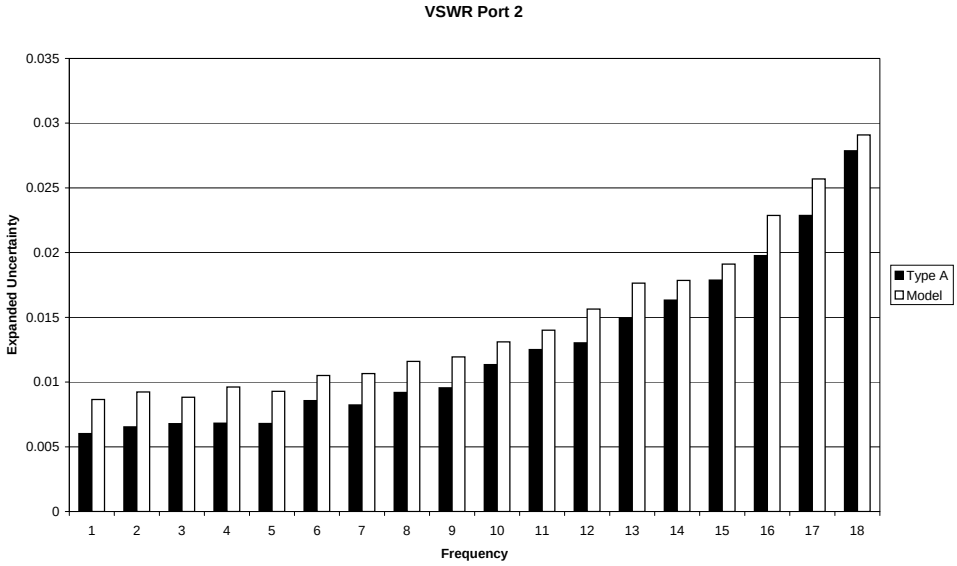

Figure 4: VSWR values for port 2.

Table 5: VSWR at splitter port 2: type A uncertainties.

f	VSWR	U	dof	k
1	1.012615	0.006021	269	1.97
2	1.015358	0.006545	225	1.97
3	1.014301	0.006783	120	1.98
4	1.014624	0.006823	78	1.99
5	1.023685	0.006805	61	2.00
6	1.027024	0.008570	38	2.02
7	1.024279	0.008235	32	2.04
8	1.014710	0.009203	24	2.07
9	1.018026	0.009552	23	2.07
10	1.040957	0.011355	20	2.09
11	1.040193	0.012517	16	2.13
12	1.046631	0.013027	14	2.16
13	1.040110	0.014965	14	2.16
14	1.030486	0.016327	15	2.13
15	1.024673	0.017875	15	2.13
16	1.045429	0.019768	14	2.15
17	1.068475	0.022870	13	2.16
18	1.042214	0.027866	14	2.16

Table 6: VSWR at splitter port 2: model uncertainties.

f	VSWR	U	dof	k
1	1.012615	0.008650	892	1.96
2	1.015358	0.009236	740	1.96
3	1.014301	0.008823	485	1.96
4	1.014624	0.009618	304	1.97
5	1.023685	0.009284	214	1.97
6	1.027024	0.010503	152	1.98
7	1.024279	0.010658	98	1.98
8	1.014710	0.011594	69	1.99
9	1.018026	0.011945	65	2.00
10	1.040957	0.013104	45	2.01
11	1.040193	0.014009	31	2.04
12	1.046631	0.015639	37	2.03
13	1.040110	0.017643	35	2.03
14	1.030486	0.017849	31	2.04
15	1.024673	0.019119	25	2.06
16	1.045429	0.022876	32	2.04
17	1.068475	0.025687	25	2.06
18	1.042214	0.029093	19	2.09

The expanded uncertainties for the VSWR values measured at splitter port 3 are shown in Fig. 5, the corresponding numerical data is reported in Tables 7 and 8, together with the calculated value, effective degrees-of-freedom and the k factor.[13]

The agreement between the two methods of uncertainty estimation for the VSWR data is better than it was for the $\boldsymbol{E}_{\mathrm{S}}$ measurements at the same port (Fig. 3). The type A uncertainties still tend to dominate the model-based ones at higher frequencies, which again is the reverse of the port 2 behaviour. However, there is really only one point where this difference is marked, at 17 GHz.

As already noted for the $\boldsymbol{E}_{\mathrm{S}}$ measurements at port 3, an increase in expanded uncertainty appears to correlate with a fall in the number of degrees-of-freedom. We attribute the better agreement in this case to the fact that we are estimating a scalar quantity. Effectively, there is more information available for a scalar estimate from the same set of raw measurements, allowing a less conservative uncertainty to be assigned.

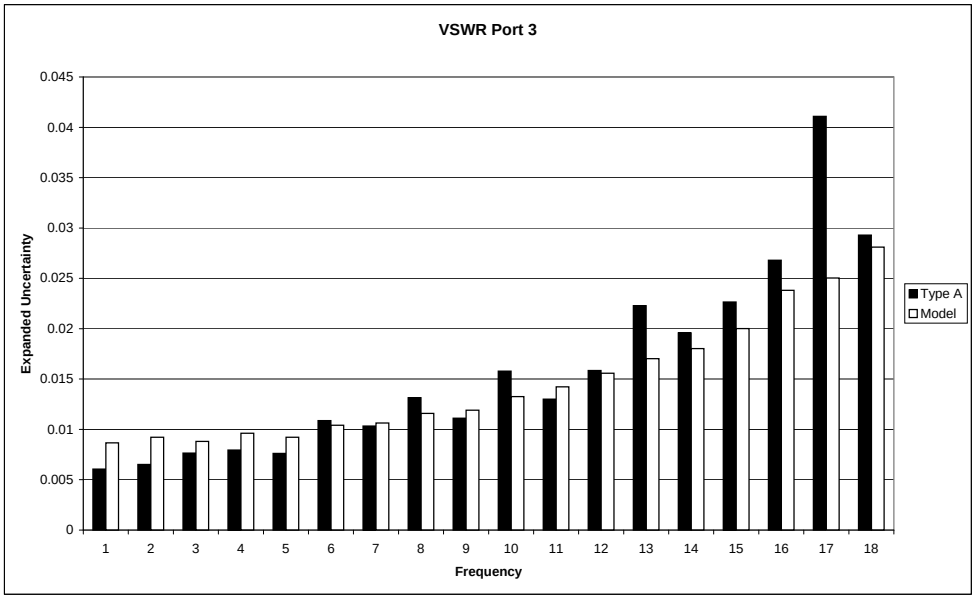

Figure 5: VSWR values for port 3.

[13]Note that VSWR is a scalar quantity, so the expanded uncertainty is calculated here according to the *Guide*, the k factor is determined from the t-distribution, etc.

Table 7: VSWR at splitter port 3: type A uncertainties.

f	VSWR	U	dof	k
1	1.013632	0.006058	269	1.97
2	1.013921	0.006513	224	1.97
3	1.012997	0.007640	41	2.02
4	1.013109	0.007941	51	2.01
5	1.017899	0.007611	51	2.01
6	1.020199	0.010866	16	2.13
7	1.025426	0.010328	22	2.08
8	1.016408	0.013151	14	2.15
9	1.014786	0.011107	20	2.09
10	1.054122	0.015782	11	2.20
11	1.058709	0.013002	17	2.12
12	1.041381	0.015853	16	2.12
13	1.005127	0.022278	10	2.26
14	1.048382	0.019588	17	2.11
15	1.072402	0.022647	15	2.15
16	1.076955	0.026797	13	2.16
17	1.042765	0.041095	9	2.26
18	1.020733	0.029295	16	2.13

Table 8: VSWR at splitter port 3: model uncertainties.

f	VSWR	U	dof	k
1	1.013632	0.008659	892	1.96
2	1.013921	0.009220	740	1.96
3	1.012997	0.008812	485	1.96
4	1.013109	0.009617	305	1.97
5	1.017899	0.009227	214	1.97
6	1.020199	0.010408	151	1.98
7	1.025426	0.010637	97	1.98
8	1.016408	0.011589	68	2.00
9	1.014786	0.011901	65	2.00
10	1.054122	0.013254	44	2.01
11	1.058709	0.014232	31	2.04
12	1.041381	0.015573	37	2.03
13	1.005127	0.017028	35	2.03
14	1.048382	0.018030	31	2.04
15	1.072402	0.020020	24	2.07
16	1.076955	0.023816	32	2.04
17	1.042765	0.025034	25	2.06
18	1.020733	0.028099	19	2.09

3.4 Reflection coefficient measurements at the splitter port

Reflection coefficient measurements have been made using the free port of the splitter as a reflectometer. The values of $\boldsymbol{E}_{\mathrm{S}}$, $\boldsymbol{E}_{\mathrm{R}}$ and $\boldsymbol{E}_{\mathrm{D}}$ obtained during calibration are used to correct the raw measurement data obtained at the splitter port (see section 2.2).

We have measured the voltage reflection coefficient of a 50 dB attenuator and subtracted this value from a one determined at NPL. The covariance for the difference was used to calculate a normalised 'statistical distance' from the origin. If the statistical distance is less than unity, it means that the origin lies inside the perimeter of the 95% region of uncertainty for the difference. If the uncertainties are accurately evaluated then, on average, about 5% of points are expected to fall outside the region of uncertainty.

Figure 6 shows the results for measurements made at port 2 with the numerical data presented in Tables 9 and 10. Note that the difference values in these tables are expressed in polar coordinates, with the angle given in degrees.

One out of the eighteen frequency points for the type A data lies just outside the 95% region of uncertainty and all of the model uncertainty points are contained within. There appears to be a reasonably even distribution of distances over the range. These results show consistency between our measurements at the splitter port and the NPL values. The model uncertainties may be slightly conservative.

Table 9: Difference of measured VRC at port 2 with type A uncertainties.

f	difference	U	e	dof	k
1	(0.001703,-166)	0.475129	0.04	169	2.48
2	(0.000447,-117)	0.109220	0.16	190	2.47
3	(0.000774,-78)	0.182054	0.40	124	2.49
4	(0.000352,63)	0.087991	0.43	110	2.49
5	(0.000428,80)	0.105225	0.42	94	2.50
6	(0.000551,-162)	0.131641	0.56	33	2.61
7	(0.000782,-115)	0.145660	0.68	25	2.67
8	(0.001990,-31)	0.506581	0.47	61	2.53
9	(0.000389,-13)	0.096359	0.43	79	2.51
10	(0.000465,89)	0.053095	0.84	9	3.28
11	(0.001924,-61)	0.500132	0.64	30	2.62
12	(0.004243,-105)	1.080568	0.52	49	2.55
13	(0.003663,-118)	0.557932	0.88	7	3.45
14	(0.003220,-146)	0.525679	0.61	12	3.00
15	(0.003983,-165)	0.490829	0.51	9	3.27
16	(0.002597,123)	0.451763	0.58	16	2.80
17	(0.003278,-153)	0.409034	0.58	11	3.06
18	(0.004886,-160)	0.726465	0.74	12	3.00

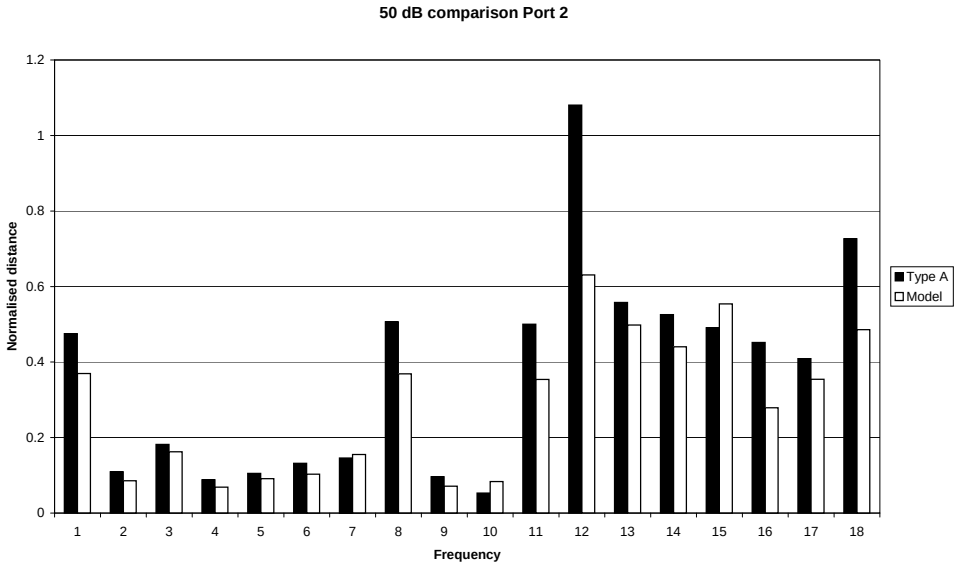

Figure 6: The difference between $\mathbf{\Gamma}$ as measured at port 2 of the splitter with the value determined at NPL. The vertical axis is a normalised 'statistical distance' from the origin in the complex plane.

Table 10: Difference of measured VRC at port 2 with model uncertainties.

f	difference	U	e	dof	k
1	(0.001703,-166)	0.369582	0.00	398	2.46
2	(0.000447,-117)	0.085503	0.00	435	2.46
3	(0.000774,-78)	0.162186	0.00	407	2.46
4	(0.000352,63)	0.068844	0.00	536	2.46
5	(0.000428,80)	0.091091	0.00	440	2.46
6	(0.000551,-162)	0.103041	0.00	659	2.46
7	(0.000782,-115)	0.155188	0.00	591	2.46
8	(0.001990,-31)	0.368660	0.00	570	2.46
9	(0.000389,-13)	0.071316	0.00	594	2.46
10	(0.000465,89)	0.083611	0.00	549	2.46
11	(0.001924,-61)	0.353811	0.00	571	2.46
12	(0.004243,-105)	0.630527	0.00	718	2.45
13	(0.003663,-118)	0.498269	0.00	1022	2.45
14	(0.003220,-146)	0.440463	0.00	825	2.45
15	(0.003983,-165)	0.554090	0.00	487	2.46
16	(0.002597,123)	0.278784	0.00	569	2.46
17	(0.003278,-153)	0.354471	0.00	502	2.46
18	(0.004886,-160)	0.485914	0.00	115	2.49

Figure 7 shows the results for measurements made at port 3. The numerical data is presented in Tables 11 and 12.[14]

In this case, none of the distances exceeds unity. The deviations of the type A data are noticeably less than the model data above 6 GHz, suggesting that the type A uncertainty estimate here could be a little conservative. Again, it is hard to be sure with the small set of data available.

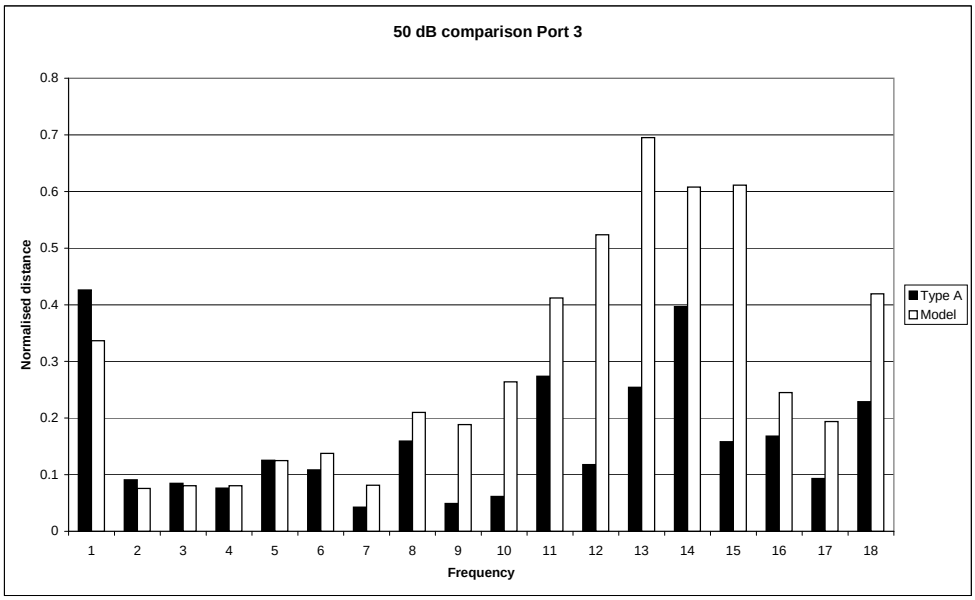

Figure 7: The difference between $\mathbf{\Gamma}$ as measured at port 3 of the splitter with the value determined at NPL. The vertical axis is a normalised 'statistical distance' from the origin in the complex plane.

[14]Note that difference data in these tables are expressed in polar coordinates, with the angle in degrees.

Table 11: Difference of measured VRC at port 3 with type A uncertainties.

f	difference	U	e	dof	k
1	(0.001551,-158)	0.426134	0.18	170	2.48
2	(0.000396,-11)	0.090977	0.34	159	2.48
3	(0.000384,-124)	0.084813	0.56	53	2.55
4	(0.000414,-167)	0.076248	0.66	28	2.64
5	(0.000586,-124)	0.125383	0.38	36	2.59
6	(0.000733,-75)	0.108372	0.65	14	2.89
7	(0.000408,16)	0.042539	0.82	8	3.29
8	(0.001129,15)	0.159254	0.90	6	4.11
9	(0.001024,179)	0.049118	0.94	5	4.92
10	(0.001465,-93)	0.061471	0.96	5	4.90
11	(0.002239,-50)	0.273728	0.97	5	4.94
12	(0.003509,-76)	0.117906	0.97	4	4.96
13	(0.005123,-150)	0.254243	0.96	5	4.93
14	(0.004445,-142)	0.396782	0.91	5	4.90
15	(0.004350,-158)	0.158382	0.94	5	4.91
16	(0.002284,170)	0.168026	0.91	5	4.12
17	(0.001791,-178)	0.093354	0.86	5	4.92
18	(0.004206,-176)	0.228823	0.91	6	4.12

Table 12: Difference of measured VRC at port 3 with model uncertainties.

f	difference	U	e	dof	k
1	(0.001551,-158)	0.336494	0.00	398	2.46
2	(0.000396,-11)	0.075797	0.00	434	2.46
3	(0.000384,-124)	0.080533	0.00	406	2.46
4	(0.000414,-167)	0.080672	0.00	541	2.46
5	(0.000586,-124)	0.124963	0.00	439	2.46
6	(0.000733,-75)	0.137636	0.00	651	2.46
7	(0.000408,16)	0.081259	0.00	583	2.46
8	(0.001129,15)	0.210005	0.00	564	2.46
9	(0.001024,179)	0.188560	0.00	591	2.46
10	(0.001465,-93)	0.263980	0.00	549	2.46
11	(0.002239,-50)	0.412059	0.00	574	2.46
12	(0.003509,-76)	0.523614	0.00	719	2.45
13	(0.005123,-150)	0.695178	0.00	1032	2.45
14	(0.004445,-142)	0.607812	0.00	834	2.45
15	(0.004350,-158)	0.611317	0.00	478	2.46
16	(0.002284,170)	0.245101	0.00	571	2.46
17	(0.001791,-178)	0.193900	0.00	508	2.46
18	(0.004206,-176)	0.419222	0.00	114	2.49

4 Discussion

As stated in the Introduction, the main reason for undertaking this project was to gain experience in applying the rigorous mathematical procedure described in Section 1.2. That procedure is an extension of the now well-established scalar procedure described in the *Guide* [2]. So, it is of particular interest to the measurement community as a way of harmonizing uncertainty calculations in complex quantities. This work was undertaken as a 'case study', looking at the practicality of the approach.

It has been a moderately complicated computational exercise, involving the solution of simultaneous equations, as well as handling a large number of uncertain input quantities influencing the measurement. The mathematics tends to be rather more laborious in complex-valued problems, because there are more terms to handle, more partial derivatives to calculate, and matrix expressions to manipulate.

Software has been used to handle this difficulty. The software is general-purpose and could easily be applicable to other RF measurement problems. It automatically propagates uncertainty contributions as well as determining any correlations that arise as a result of calculations. This means that results can be compared and used in subsequent calculations, which is a significant advantage. These are the same benefits afforded by the techniques established for scalar uncertainty calculations.

For example, in this work, the three error-correction parameters for a one-port reflectometer have been determined, *including* the correlations between them. This information was used to measure reflection coefficients at the splitter port and finally the measured reflection coefficients were compared with calibration data. Throughout, we were able to maintain complete uncertainty information. Alternative approaches to VNA uncertainty assessment, such as the well-known 'ripple technique' simply cannot offer this rigor and flexibility.

One of the appealing aspects of the mathematical procedure for complex values is that it reverts to the scalar procedure for a scalar measurand. We have reported values of effective VSWR, which is a scalar quantity associated with the complex value of effective source match. Without any adjustment, our calculations adhered strictly to the *Guide* when dealing with the VSWR, yet the same framework supported the calculations for complex reflection coefficients.

The project became more ambitious than first planned when a model of VNA measurement uncertainty was developed as an alternative way to estimate measurement uncertainty. Fortunately, the results obtained indicate that this approach is well-founded and appears practical. We feel that this success merits further attention, as it appears to offer a robust route to traceability for VNA measurements. More work is needed to decide how to establish the parameter values for components of uncertainty in such models.

5 Conclusions

This study has found it feasible to apply the new complex-value form of the law of propagation of uncertainty [1] to assess measurement uncertainty in values of effective source match and VSWR for a power splitter measured using the Direct Method.

The study, nevertheless, relied on new software that supports the mathematical procedure for propagating uncertainty. The calculations would have been onerous without this software. Indeed, such software may even encourage uptake of the associated mathematical procedure.

The study has compared two methods of attributing input uncertainty contributions to the actual measurements. One is based on a type A assessment of repeated measurements, the other is based on modelling of uncertainties. Both appear to adequately represent the input contributions in the final assessment of measurement uncertainty adequately. Strong evidence for this comes from measurements of a calibrated verification standard.

The initial success of using a signal flow model of VNA measurement uncertainty could probably be improved on by better estimates for model parameters of VNA performance. The VNA model could also be extended by incorporating error correction formulae, which would then provide full uncertainty statements for $\boldsymbol{S}$-parameter measurements on a *calibrated* VNA. This would appear to provide a robust route to traceable VNA measurements.

A VNA uncertainty

The accurate modelling of uncertainty contributions from a VNA is quite complicated. A detailed report has been prepared by Vidkjaer, of Denmark Technical University [10].[15] Another source of information is a recent paper by Rytting, of Agilent [11].

Our attempts to account quantitatively for VNA uncertainty here are modest. Nevertheless, the modelling is an interesting part of the study. It could be easily extended to handle measurments with a calibrated VNA as well.

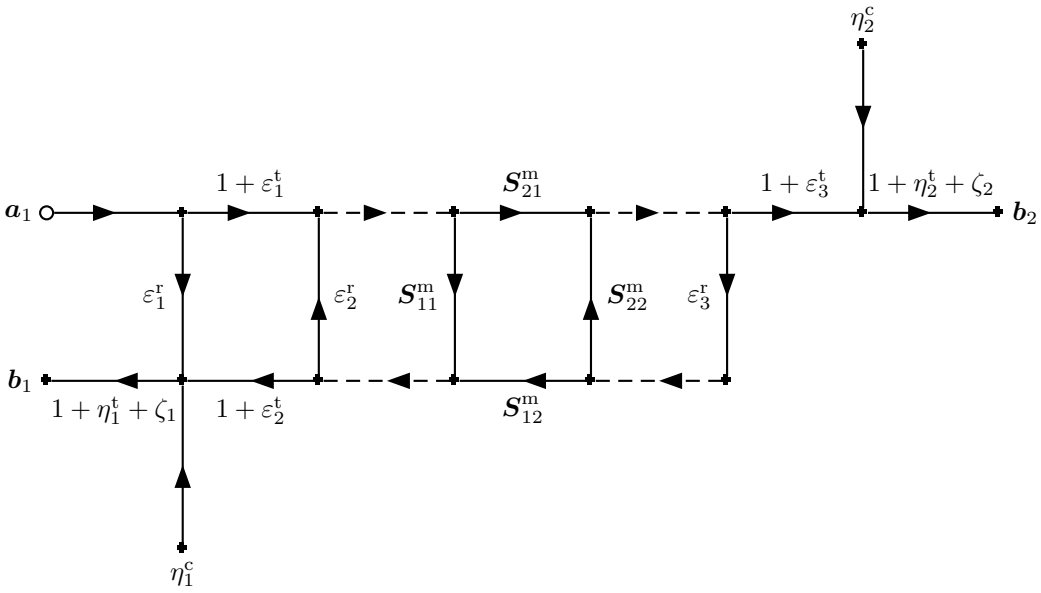

Figure 8: A signal flow diagram for the model of VNA uncertainties used in this study. The four measured *raw* $\boldsymbol{S}$-parameters of a device are shown in the centre of the figure. To the left and right of this are 2-port segments introducing cable and connector repeatability and stability uncertainties, represented by the ε terms. Uncertainty due to noise, drift, and stability are modelled by η^{t}, for uncertainties proportional to signal, and by η^{c}, for any constant terms (e.g., noise floor). Uncertain errors in linearity are represented by the ζ terms.

Figure 8 shows a signal flow diagram of the model used for VNA uncertainty. Non-ideal connector and cable behaviour introduces uncertainty to any measurement of $\boldsymbol{S}$-parameters, so we place the measured raw $\boldsymbol{S}$-parameter values between a pair of 2-port networks that model this. The branches in these networks are assigned nominal values of unity, for transmission, and zero for reflection; the ε terms represent the standard uncertainties associated with these values. This slightly unconventional

[15] We are grateful to Dr. Simon, of Rhode & Schwartz, for showing us a copy.

notation means, for instance, that a signal passing along a transmission branch does not change in value, but gains an additional component of uncertainty.

Raw VNA measurements are subject to random noise and departures from linearity. These are represented by the η and ζ terms, some of which contribute in proportion to the signal value (η^{t}) and others, such as noise floor, add directly to the signal uncertainty (η^{c}).

The VNA uncertainty model is used in the following way. For every set of $\boldsymbol{S}$-parameters measured, a corresponding set of uncertain numbers is generated with uncertainty contributions based on the signal flow model. The set of four $\boldsymbol{S}$-parameters for a particular two-port VNA measurement will depend on the twelve uncertainty terms shown in Figure 8. In some cases, a term is intended to be 'common' to the set, such as the connector uncertainties, while others, like noise, are assumed to be random and independent for each parameter; some, like the dynamic accuracy (linearity) are considered a residual systematic error of the VNA. Nuances like these are handled by the way in which the software model defines terms.

A.1 VNA uncertainty values

Values for the uncertainty terms used in this work are shown below. They are estimates based on measurements of VNA performance. However, in assigning them to the model a few arbitrary assumptions have been made.

- Cable and connector stability and repeatability: $\varepsilon^{\mathrm{t}} = 0.002$ and $\varepsilon^{\mathrm{r}} = 0.0005$;
- Noise floor: $\eta^{\mathrm{c}} = 20 \times 10^{-}6$ V (rms);
- Trace noise: $\eta^{\mathrm{t}} = 0.003$ dB;
- Linearity: $\zeta = 0.008(1 + 0.1x)$ dB, where x is the attenuation in dB.

Uncertainties given in dB are converted to a relative uncertainty on a linear scale

$$u_{\mathrm{lin}}/|x| = \left(10^{\frac{u_{\mathrm{dB}}}{20}} - 1\right) \ , \tag{11}$$

where $|x|$ is the magnitude of the associated complex amplitude.

Arbitrarily, each term has been assigned fifty degrees-of-freedom.

B Effective degrees-of-freedom

The notion of degrees-of-freedom arises when an input quantity estimate is based on a small number of repeated measurements. For scalar quantities, there is a procedure for estimating the degrees-of-freedom of a result, given degrees-of-freedom for the inputs [2]. In the complex case, we have chosen to use a simple algorithm suggested recently [8]. The calculation is as follows.

First, evaluate the set of covariance matrices

$$\mathbf{V}_i(\boldsymbol{y}) = \mathbf{U}_i(\boldsymbol{y})\,\mathbf{R}_{ij}(\mathbf{X})\,\mathbf{U}_j(\boldsymbol{y})'\,, \tag{12}$$

where i ranges over the input quantities and

$$\mathbf{R}_{ij}(\mathbf{X}) = \begin{bmatrix} r(x_{1i}, x_{1j}) & r(x_{1i}, x_{2j}) \\ r(x_{2i}, x_{1j}) & r(x_{2i}, x_{2j}) \end{bmatrix} \tag{13}$$

is the matrix of correlation coefficients between the components of the inputs $\boldsymbol{x}_i$ and $\boldsymbol{x}_j$.

Then calculate the following values ($v_{i\cdot jk}$ is the jk^{th} element of matrix $\mathbf{V}_i$)

$$\begin{aligned} A &= 2\left(\sum v_{i\cdot 11}\right)^2 \\ D &= \sum v_{i\cdot 11} \sum v_{i\cdot 22} + \left(\sum v_{i\cdot 12}\right)^2 \\ F &= 2\left(\sum v_{i\cdot 22}\right)^2 \end{aligned}$$

and (ν_i is the degrees-of-freedom associated with the i^{th} input)

$$\begin{aligned} a &= 2\sum v_{i\cdot 11}^2/\nu_i \\ d &= \sum \left(v_{i\cdot 11}\, v_{i\cdot 22} + v_{i\cdot 12}^2\right)/\nu_i \\ f &= 2\sum v_{i\cdot 22}^2/\nu_i\,. \end{aligned}$$

Finally, the effective degrees-of-freedom is

$$\nu_{\text{eff}} = \frac{A + D + F}{a + d + f}\,. \tag{14}$$

It is worth noting that when $\boldsymbol{y}$ happens to be real-valued (e.g., a VSWR) this calculation is equivalent to the usual scalar one, sometimes referred to as the Welch-Satterthwaite formula [2].

C More on uncertainty reporting

Often when reporting the measurement uncertainty in a scalar quantity an uncertainty budget is given (e.g. Appendix H in [2]). This may serve two purposes. It helps to assess the relative importance of different contributions to the combined measurement uncertainty and it may also provide enough information to allow a result to be combined or compared with other measurement results (e.g., contributions to the combined uncertainty in one measurement may be shared with others, leading to correlation).

Two of the parameters usually reported in an uncertainty budget are sensitivity coefficients and components of uncertainty. These familiar concepts for scalar uncertainty can be generalised to the complex case. However, both are represented as (2×2) matrices, which is not a convenient form for quick interpretation of results. This section looks at these extensions and proposes scalar summary values that are more convenient for qualitative comparison. To illustrate their use, we investigate the contributions to uncertainty for the results of the port 3 measurements.

C.1 Complex sensitivity coefficients

When considering the contributions to uncertainty in a scalar quantity it is convenient to estimate the sensitivity of a measurement function to variations in input values. This leads to a set of 'sensitivity coefficients' for a measurement, which are the partial derivatives of the measurement function with respect to its inputs

$$c_j = \frac{\partial f(y)}{\partial x_j} \,. \tag{15}$$

The complex extension of this is the partial derivative

$$\boldsymbol{c}_j = \frac{\partial \boldsymbol{f}(\boldsymbol{y})}{\partial \boldsymbol{x}_j} \,, \tag{16}$$

which is actually the equivalent of the Jacobian matrix

$$\mathbf{J}_j(\boldsymbol{y}) = \begin{bmatrix} \frac{\partial f_1}{\partial x_{1j}} & \frac{\partial f_1}{\partial x_{2j}} \\ \frac{\partial f_2}{\partial x_{1j}} & \frac{\partial f_2}{\partial x_{2j}} \end{bmatrix} \,. \tag{17}$$

$\mathbf{J}_j(\boldsymbol{y})$ is the Jacobian matrix of $\boldsymbol{f}$ with respect to the input $\boldsymbol{x}_j$; the matrix elements are scalar sensitivities of the real and imaginary components.

The (2×2) Jacobian matrices can be related to the complex partial derivatives of $\boldsymbol{f}$ by a simple and elegant matrix representation for complex numbers. For any complex $\boldsymbol{z} \equiv a + \mathrm{j}\, b$ the mapping

$$\mathbf{M}(\boldsymbol{z}) \equiv \begin{bmatrix} a & -b \\ b & a \end{bmatrix} \tag{18}$$

generates a (2×2) matrix for $\boldsymbol{z}$. Such matrices behave as complex numbers under the usual matrix operations for arithmetic: division corresponds to multiplication by the matrix inverse, and taking the matrix transpose corresponds to the complex conjugate operation. Furthermore, if a complex function $\boldsymbol{f}(\boldsymbol{z})$ is analytic in the region of interest, the Cauchy-Riemann relations will apply to its partial derivatives [9], so

$$\frac{\partial f_1}{\partial a} = \frac{\partial f_2}{\partial b} \,, \; \frac{\partial f_1}{\partial b} = -\frac{\partial f_2}{\partial a} \,. \tag{19}$$

C.1.1 Summary values

The complex partial derivatives $\frac{\partial \boldsymbol{f}}{\partial \boldsymbol{x}_j}$, or the Jacobian matrices, $\mathbf{J}_j(\boldsymbol{y})$, play the role of sensitivity coefficients for a complex measurement function. However, the phase information they contain is not usually needed to assess the relative importance of the different terms in a measurement equation.

The *magnitude* of the complex derivative, or equivalently the square root of the determinant of the Jacobian matrix, can be useful in reporting sensitivity coefficients.

C.2 Components of uncertainty

A scalar sensitivity coefficient can be weighted by an input's standard uncertainty to obtain the contribution to the combined uncertainty of a result

$$u_j(y) = c_j\, u(x_j) = \frac{\partial f(y)}{\partial x_j}\, u(x_j)\ , \tag{20}$$

where $u(x_j)$ is the standard uncertainty of x_j. $u(x_j)$ has the same units as y and is usually easy to interpret as a contribution to the overall uncertainty.

In the complex case, a Jacobian sensitivity matrix can be weighted by the uncertainty in the associated input value. The elements of the resulting matrix will be combined in the covariance matrix for the result.

The weighted Jacobian matrix is obtained by simple multiplication

$$\mathbf{U}_j(\boldsymbol{y}) \equiv \begin{bmatrix} u_{1\cdot 1j} & u_{1\cdot 2j} \\ u_{2\cdot 1j} & u_{2\cdot 2j} \end{bmatrix} \tag{21}$$

$$= \begin{bmatrix} \frac{\partial f_1}{\partial x_{1j}} & \frac{\partial f_1}{\partial x_{2j}} \\ \frac{\partial f_2}{\partial x_{1j}} & \frac{\partial f_2}{\partial x_{2j}} \end{bmatrix} \begin{bmatrix} u(x_{1j}) & 0 \\ 0 & u(x_{2j}) \end{bmatrix}\ , \tag{22}$$

where $u(x_{1j})$ and $u(x_{2j})$ are the standard uncertainties in the real and imaginary components of $\boldsymbol{x}_j$, respectively.

This report refers to $\mathbf{U}_j(\boldsymbol{y})$ as a *component of uncertainty* matrix. Note that $\mathbf{U}_j(\boldsymbol{y})$ is not a covariance matrix nor is it symmetric. A component-of-uncertainty matrix can be calculated for each input to the measurement function.

It is useful to consider how the elements of the final covariance matrix for a result are related to the elements in the component-of-uncertainty matrices. In the simplest scenario, all inputs can be assumed independent and the covariance matrix becomes

$$\mathbf{V}(\boldsymbol{y}) = \begin{bmatrix} \sum_{j=1}^{m}\sum_{i=1}^{2} u_{1\cdot ij}^2 & \sum_{j=1}^{m}\sum_{i=1}^{2} u_{1\cdot ij}u_{2\cdot ij} \\ \sum_{j=1}^{m}\sum_{i=1}^{2} u_{1\cdot ij}u_{2\cdot ij} & \sum_{j=1}^{m}\sum_{i=1}^{2} u_{2\cdot ij}^2 \end{bmatrix}\ . \tag{23}$$

A more realistic scenario would consider that the real and imaginary components of inputs could also be correlated. The first and second diagonal elements of $\mathbf{V}(\boldsymbol{y})$

then become, respectively,

$$\sum_{j=1}^{n}\left[\left(\sum_{i=1}^{2} u_{1\cdot ij}^2\right) + 2\, r(x_{1j}, x_{2j})\, u_{1\cdot 1j} u_{1\cdot 2j}\right] \tag{24}$$

$$\sum_{j=1}^{n}\left[\left(\sum_{i=1}^{2} u_{2\cdot ij}^2\right) + 2\, r(x_{1j}, x_{2j})\, u_{2\cdot 1j} u_{2\cdot 2j}\right] \tag{25}$$

and the off-diagonal elements are equal to

$$\sum_{j=1}^{n}\left[\sum_{i=1}^{2} u_{1\cdot ij} u_{2\cdot ij} + r(x_{1j}, x_{2j})\,(u_{1\cdot 2j} u_{2\cdot 1j} + u_{1\cdot 1j} u_{2\cdot 2j})\right] . \tag{26}$$

C.2.1 Summary values

The square root of the sum of the squares of the four elements in a component-of-uncertainty matrix, u^{rms}, has the same units as the measurand and contributes directly to the diagonal terms of the covariance matrix. Indeed, the Total Variance, which is a standard summary value for variance-covariance matrices used in applied statistics [4], can be evaluated as the sum of the squares of all the u^{rms} values for a particular result.

C.3 A closer look at the port 3 results

Section 3 noted that the uncertainty statements for some measurements at splitter port 3, obtained using the type A approach, showed a distinct increase compared to the model-based assessment of uncertainty for at the same points. The data presented in Section 3 suggested that this behaviour could be attributed to greater variation in the small number of measurements. As an exercise in the use of the summary value representations given above, this section will look at the individual contributions to uncertainty in these measurements.

C.3.1 Contributions to the uncertainty in $\boldsymbol{E}_{\mathrm{S}}$

We first consider the sensitivities and components of uncertainty for the measurement of $\boldsymbol{E}_{\mathrm{S}}$. The three frequency points: 6 GHz, 11 GHz and 17 GHz have been chosen for reporting.

Sensitivities depend only on the measurement equation. There are six inputs so there are six sensitivities. The results in Table 13 are copied from the computer screen, with a little editing to improve readability. They show that all six inputs are reasonably well-balanced in their contributions to uncertainty in the result, although the type A measurement of the load is most critical.

Table 13: Input sensitivities for $\boldsymbol{E}_{\mathrm{S}}$.

```
----------------------------------
Sensitivities for E_S at 6GHz

'uid(7)::load_std':        1.015
'uid(28)::open_std':       0.506
'uid(49)::short_std':      0.511
'uid(109)::Type-A load':   1.652
'uid(111)::Type-A open':   0.833
'uid(113)::Type-A short':  0.825
----------------------------------
Sensitivities for E_S at 11GHz

'uid(14)::load_std':       1.001
'uid(35)::open_std':       0.500
'uid(56)::short_std':      0.517
'uid(97)::Type-A load':    1.656
'uid(99)::Type-A open':    0.829
'uid(101)::Type-A short':  0.845
----------------------------------
Sensitivities for E_S at 17GHz

'uid(9)::load_std':        1.024
'uid(30)::open_std':       0.525
'uid(51)::short_std':      0.520
'uid(157)::Type-A load':   1.992
'uid(159)::Type-A open':   1.004
'uid(161)::Type-A short':  1.057
----------------------------------
```

Table 14: Type A components of uncertainty (rms) for $\boldsymbol{E}_{\mathrm{S}}$ measured at port 3.

```
 ---------------------------------
Components of E_S at 6GHz

 'uid(7)::load_std':        0.00155
 'uid(28)::open_std':       0.00143
 'uid(49)::short_std':      0.00145
 'uid(109)::Type-A load':   0.00157
 'uid(111)::Type-A open':   0.00038
 'uid(113)::Type-A short':  0.00138
 ---------------------------------
Components of E_S at 11GHz

 'uid(14)::load_std':       0.00147
 'uid(35)::open_std':       0.00254
 'uid(56)::short_std':      0.00242
 'uid(97)::Type-A load':    0.00433
 'uid(99)::Type-A open':    0.00246
 'uid(101)::Type-A short':  0.00139
 ---------------------------------
Components of E_S at 17GHz

 'uid(9)::load_std':        0.00190
 'uid(30)::open_std':       0.00410
 'uid(51)::short_std':      0.00503
 'uid(157)::Type-A load':   0.00558
 'uid(159)::Type-A open':   0.00291
 'uid(161)::Type-A short':  0.00482
 ---------------------------------
```

The sensitivities of $\boldsymbol{E}_{\mathrm{S}}$ to the three standards has been worked out analytically ([10, Eq 113] and [12, Eq 16]) in the approximation of a perfect load, so it is possible to check the magnitude of these results. The values expected are close to: 1.0, 0.5 and 0.5, for the load, open and short respectively. The sensitivity to measured values also have analytic expressions (again for a perfect load) [10, Eq (117)]. They depend on the measured values and parameter estimates, but we find good agreement with the results above.

The rms summaries of the component of uncertainty terms in the port 3 measurement is summarised in Table 14. These results show that the type A measurement uncertainties grew substantially at the higher frequencies compared to 6 GHz, which show negligible difference between type A and model uncertainties. However, they do not seem out of proportion with the uncertainties attributed to the calibration standards.

As a comparison, the set of data in Table 15 reports the rms summaries of the components of uncertainty in the port 2 measurements. Here we see much smaller uncertainty contributions from the type A assessment of uncertainty.

Clearly, the variability in the type A uncertainty estimates is causing the behaviour observed. However, it is still difficult to know whether or not there is a problem with

Table 15: Type A components-of-uncertainty (rms) for $\boldsymbol{E}_{\mathrm{S}}$ measured at port 2.

```
 ---------------------------------
Components of E_S at 6GHz

 'uid(7)::load_std':        0.00155
 'uid(28)::open_std':       0.00143
 'uid(49)::short_std':      0.00145
 'uid(109)::Type-A load':   0.00094
 'uid(111)::Type-A open':   0.00053
 'uid(113)::Type-A short':  0.00069
 ---------------------------------
Components of E_S at 11GHz

 'uid(14)::load_std':       0.00147
 'uid(35)::open_std':       0.00253
 'uid(56)::short_std':      0.00244
 'uid(97)::Type-A load':    0.00068
 'uid(99)::Type-A open':    0.00067
 'uid(101)::Type-A short':  0.00087
 ---------------------------------
Components of E_S at 17GHz

 'uid(9)::load_std':        0.00191
 'uid(30)::open_std':       0.00425
 'uid(51)::short_std':      0.00490
 'uid(157)::Type-A load':   0.00183
 'uid(159)::Type-A open':   0.00111
 'uid(161)::Type-A short':  0.00129
 ---------------------------------
```

the measurements given the small amount of data available. Further investigation is really called for.

References

[1] N. M. Ridler and M. J. Salter, *"An approach to the treatment of uncertainty in complex S-parameter measurements"* Metrologia, **39** (2002) 295-302.

[2] *Guide to the Expression of Uncertainty in Measurement*, (International Organisation for Standardization, Geneva, 1995).

[3] J. R. Juroshek, *"A direct calibration method for measuring equivalent source mismatch"*, Microwave J., **40**(10), (1997) 106-118.

[4] B. D. Hall, *"On the propagation of uncertainty in complex-valued quantities"* Metrologia, **41** (2004) 173-177.

[5] B. D. Hall, *"A computational technique for evaluating and propagating the uncertainty of complex valued quantities"*, Proceedings of 60th ARFTG (Washington DC, USA, Dec 5-6), (2002), 19-28.

[6] W. H. Press, S. A. Teukolsky, W. T. Vetterling and B. P. Flannery, *"Numerical Recipies in C"*, 2nd Ed., (Cambridge University Press, 1992).

[7] The general-purpose software used in this work for uncertainty calculation is an example of the 'GUM Tree' design technique. More information is available at `http:\\www.irl.cri.nz\msl\mst`. Two versions for complex numbers are available: one in C++, the other in Python. The software is free but subject to an 'evaluation licence' agreement. We would like to encourage ANAMET members to try the software, so if there are any concerns about accepting the licence agreement, please contact us through the email address on the web.

[8] R. Willink and B. D. Hall, *"A classical method for uncertainty analysis with multidimensional data"*, Metrologia, **39** (2002) 361-369.

[9] M. R. Spiegel, *Complex variables*, (Schaum's Outline Series, McGraw-Hill, Great Britian, 1974).

[10] J. Vidkjaer, *"Network analyzer uncertainty computations for small-signal model extractions"* (Technical University of Denmark Report, R549, Feb., 1994).

[11] D. Rytting, *"Network analyzer accuracy overview"*, Proceedings of 58th ARFTG Meeting, 2001.

[12] M. Rodriguez, *"Comparison between the ripple technique and the direct calibration method for characterisation of directional devices"*, IEE Proc.-Sci. Meas. Technol. **47** (2000) 196-201.